CrossMark

Structural, optical and photo-electrical properties of nanocrystalline ZnSe thin films

Jeewan Sharma[1] · Harinder Singh[1] · Tejbir Singh[2] · Anup Thakur[3]

Abstract

Present paper reports the effect of deposition temperature on structure and electrical conduction mechanism of ZnSe thin films. Films have been fabricated on glass substrates using condensation technique. The depositions have been performed in presence of Ar at various substrate temperatures (298–373 K). X-ray diffraction (XRD) studies reveal hexagonal structure with texture changing from (002) to (102) on increasing substrate temperature. The crystallite size (6.1–8.4 nm), strain (-0.0133 to -0.00748 $\mathrm{lin^{-2}\,m^{-4}}$), dislocation densities (1.857×10^{16}–1.015×10^{16} $\mathrm{lin\,m^{-2}}$) and stacking fault probability (0.0038–0.0041) have been calculated from XRD data. The optical gap (2.75–3.00 eV), refractive index (2.38–2.48) and ionicity (0.425–0.446) have been calculated using transmission measurements. The dark-conduction and photo-conduction behaviours have been studied in temperature range 253–358 K. The two activation energies of dark conduction have been explained using different models. The conduction mechanism has been identified based on Seto's model of thermionic emission. The barrier height (0.17–0.28 eV), impurity concentration (1.26×10^{20}–3.18×10^{20} $\mathrm{cm^{-3}}$) and surface states density (1.05×10^{14}–2.15×10^{14} $\mathrm{cm^{-2}}$) have also been calculated.

1 Introduction

Chalcogenide II–VI group semiconducting thin films have been investigated for their electrical transport properties, because of their potential in photovoltaic applications [1]. Among various binary compound semiconductors, they have direct band gap and variable degree of ionicity making them suitable candidates for high electro-mechanical and electro-optical coupling materials. The degree of ionicity of these semiconductors has been observed to be strongly dependent on size [2]. In II–VI semiconductors, there is a wide variation of energy bandgap, which makes them suitable for large range of electronic and optical applications. Additionally, these semiconductors are readily miscible, allowing a continuous "engineering" of various properties [3, 4].

✉ Jeewan Sharma
  jeewansharma29@gmail.com

1 Department of Nanotechnology, Sri Guru Granth Sahib World University, Fatehgarh Sahib 140 407, India

2 Department of Physics, Sri Guru Granth Sahib World University, Fatehgarh Sahib 140 407, India

3 Department of Basic and Applied Sciences, Punjabi University, Patiala, Punjab 147 002, India

Among II–VI group semiconductors, ZnSe is most suitable material for different light emitting diodes in visible regions [5], optoelectronic devices [6, 7], thin film transistors [8], photo electrochemical cells (PEC) [9], flat panel displays [10] etc., as its band gap lies in the solar spectrum. Various synthesis methods have been tried to fully utilize physical properties and device applications of ZnSe nanocrystals. These methods include pulse deposition [11], chemical bath deposition [12], dc/rf sputtering [13], solvothermal route [14], electro-deposition method [15] and electron beam evaporation [16]. Contemporarily, chemical methods are being used to synthesize semiconducting nanoparticles. In these methods, the crystallite size is controlled by preventing agglomeration using ligand shells. These ligand shells generally influence different properties of the nanomaterials. Therefore, we look for methods in which nanomaterials are free from ligand shells [17, 18]. As compared to other methods, Inert gas condensation is relatively simple and low cost method. This method had been widely utilized to synthesize metals and nanoclusters [19, 20].

Semiconducting ZnSe is tetrahedrally bonded compound with eight valence electrons. Its various properties depend upon charge distribution, electronic structure and bonding type. The electrostatic interaction also plays an important role in determining its properties. In addition, the optical and

electrical properties of nanomaterials can be significantly influenced with the presence of imperfections such as, dislocations, lattice distortions and stacking faults, in crystal. These imperfections also lead to the micro-strain in the crystal. During the design of a component or structure, the electrical properties of materials play a major role in selection and processing of materials. Generally, ZnSe thin films can be synthesized in two different structures (Sphalerite cubic and Hexagonal) depending upon preparation conditions. To get better performance and efficiency in devices, the optimization of various properties (electrical, dielectric and optical) of thin films are very important. Presently, we have tried to control the refractive index, dislocation density, impurity concentration and surface states density by controlling the substrate temperature which could be important for the device applications.

In present study, ZnSe thin films have been deposited using thermal evaporation in presence of Ar and characterised by X-ray diffraction (XRD), optical transmission and conductivity measurements. The effect of deposition temperature on structural (crystallite size, micro-strain, dislocation density, stacking fault probability and texture coefficient), optical (band gap, refractive index, plasmon energy and ionicity) and electrical transport (dark- and photoconductivity, activation energy, barrier height, surface state density and impurity concentration) properties of ZnSe thin films has investigated. In the studied temperature range, the electronic transport of ZnSe thin films has been explained based on the model proposed by Seto [21]. The thermionic emission of the carriers is responsible for the conduction over the grain boundaries.

2 Experimental

Melt-quenching technique was successfully used to prepare semiconducting $Zn_{25}Se_{75}$ from its constituent elements (5N) as described earlier [22]. Prior to depositions of films, the substrates were cleaned chemically and ultrasonically. The depositions were done at four different substrate temperatures (298, 323, 348 and 373 K). Ar gas (2×10^{-1} mbar) was introduced by a jet placed adjacent to the Mo boat. The substrate was kept at a height of 7 cm from the boat. Before making any measurements, the deposited samples were left in the chamber for 24 hours without disturbing so that the films attain thermodynamic equilibrium [23]. Philips PW-1610 diffractometer with CuK_α radiation ($\lambda = 1.54056$ Å) was used for crystallographic study. Optical transmission was recorded using a double beam spectrophotometer [HITACHI-330]. The conductivity behaviour of films was measured using two probe method. In present study, films with planar geometry having ~ 1.0 cm length and $\sim 8 \times 10^{-2}$ cm electrode gap were used. Indium

electrodes were pre deposited as Ohmic contacts. A tungsten lamp (200 W) was used to illuminate the sample through a glass window. Light intensity was measured to be 8450 lx using a digital MASTECH, MS6610 luxmeter. All electrical measurements were performed in a vacuum of $\sim 10^{-3}$ mbar. The measurement of current was done using digital DPM-11 picoammeter having least count 1 pA.

3 Results and discussion

Figure 1 shows the patterns obtained by XRD of all zinc selenide films. The peaks from (002), (102), (110) and (112) planes could be indexed to polycrystalline hexagonal phase of ZnSe. (002) peak is prominent in all the films and (102) peak also shows its prominence in film deposited at 373 K. Comparison of observed inter planner spacing (d) values with standard, indicates good agreement (JCPDS file no. 00-015-0105). One additional Zn peak is also observed. A broad hump in the background indicates presence of amorphous phase and glass substrate.

The texture coefficient of the crystallographic planes $T_c(hkl)$, which is the preferred orientation indicator, has been calculated by using

$$T_c(hkl) = \frac{I(hkl)/I_r(hkl)}{n^{-1} \sum_n I(hkl)/I_r(hkl)} \qquad (1)$$

where n, $I(hkl)$ and $I_r(hkl)$ represent the number of the peaks in diffraction pattern, observed peak intensity and the intensity of corresponding reference peak, respectively [24]. The values of the texture coefficient for the (002) and (102) planes are represented in Table 1. The films which are deposited at lower temperatures have higher tendency of (002) orientation. However, for higher temperature depositions
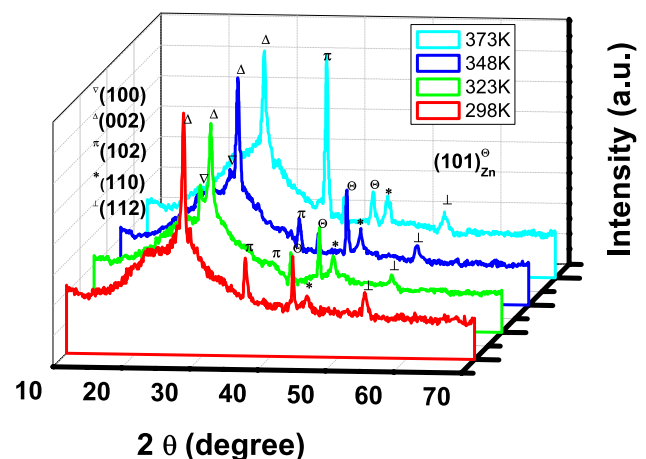

Fig. 1 X-ray diffraction patterns of all ZnSe thin films

Table 1 Structural parameters calculated from XRD patterns for all ZnSe thin films

Substrate temp. (K)	Crystallite size (nm)	Strain (lin^{-2} m^{-4})	Texture coeff.		Dislocation density (lin m^{-2})	Stacking fault probability
			(002)	(102)		
298	6.1	-1.33×10^{-2}	1.86	0.98	1.857×10^{16}	3.8×10^{-3}
323	6.7	-9.71×10^{-3}	1.78	1.00	1.618×10^{16}	4.7×10^{-3}
348	7.9	-8.68×10^{-3}	1.66	1.08	1.410×10^{16}	3.4×10^{-3}
373	8.4	-7.48×10^{-3}	1.30	1.83	1.015×10^{16}	4.1×10^{-3}

(373 K), there is a higher tendency of (102) orientation as compared to (002). The (002) texture coefficient decreases from 1.85 to 1.30 and (102) texture coefficient increases from 1.08 to 1.83 when substrate temperature increases from 298 to 373 K. Fujimura et al. [25] suggested that the crystal growth in films occur along the direction having lowest surface energy. Higher texture for (102) planes indicates that surface energy density of these planes is minimum when deposited at higher substrate temperatures.

Strain (ε) and crystallite size (L) have been calculated using Hall–Williamson method [26]

$$\beta \cos \theta = \frac{K\lambda}{L} + 4\varepsilon \sin \theta \qquad (2)$$

where β represents full width at half maximum. The values of L and ε have been calculated from $\beta \cos \theta$ versus $4 \sin \theta$ graphs as described elsewhere [27]. These values have been represented in Table 1. Transport of particles to substrate depends upon thermal gradient between the hot source and relatively cold substrate. This thermal gradient provides convection currents leading to transport of the particles to the substrate. With increase in the substrate temperature, there is decrease in thermal gradient between source and substrate. This lower thermal gradient provides more time for particles to coalesce with each other forming larger crystallites.

The films are generally strained, as there is a change in lattice parameter of films with respect to bulk. This is due to modification in nature and concentration of imperfections [28]. The strain in all the films is compressive as it is having negative value. The development of strain in polycrystalline films is due to misfit between film-substrate lattices and crystallite boundary effect [29, 30]. The variation of strain with crystallite size is represented in Table 1. The strain decreases with increasing crystallite size. In polycrystalline films, the recrystallization process is predominant at higher temperatures and there is migration of interstitial Zn atoms to grain boundaries leading to a reduction in lattice imperfections [31].

Dislocations are the imperfections in a crystal associated with the misregistry in one part of the lattice with respect to another part. The growth mechanism for ZnSe thin films is a matter of importance because it may control the dislocations. The dislocation density (δ) for these thin films has been calculated using the formula [33]

$$\delta = \frac{15\varepsilon}{aL} \qquad (3)$$

where a is lattice parameter. The calculated δ values for all thin films have been represented in Table 1. The dislocation density decreases with increase in crystallite size. From the above discussion, it is clear that at higher substrate temperature crystallite size tends to increase but micro-strain and dislocation density decrease. It is a clear indication that good quality films can be achieved at high temperatures. The stacking fault probability (α_s) for (002) planes has been calculated from the peak shift [$\Delta(2\theta)$] using [34]

$$\alpha_s = 0.253 \left[\frac{\Delta(2\theta)}{\tan \theta_{002}} \right] \qquad (4)$$

The values of α_s for the ZnSe thin films have been found to be in the range from 0.0034 to 0.0047. These values have been presented in Table 1.

The optical gap of a semiconductor can be determined if we know the absorption energy between two energy bands. The behaviour of optical absorption coefficient (α_o) with incident energy ($h\nu$) can be described by [35]

$$\alpha_o = B \frac{(h\nu - E_g)^n}{h\nu} \qquad (5)$$

where B represents a constant, E_g represents the optical gap and value of n tells about type of transition whether it is allowed/forbidden or direct/indirect [36]. In our case, the transition is allowed direct as values of n lie between 0.45 and 0.62 for all the films. In the energy range of strong absorption, the values of α_o have been calculated using the transmittance (T) curves using

$$\alpha_o = \frac{1}{t} \ln \frac{1}{T} \qquad (6)$$

where t represents sample thickness. Figure 2 shows the behavior of $(\alpha_o h\nu)^2$ with incident energy for all the films. The extrapolation of straight line portion in $(\alpha_o h\nu)^2$ curves to energy axis gives the values of E_g. In present case, the calculated band gap agrees with earlier reported values for ZnSe [31]. In a review on ZnSe thin films, Pathak and Bais [32] reported that the optical band gap of ZnSe thin films deposited by various methods, ranges between 1.60–2.82
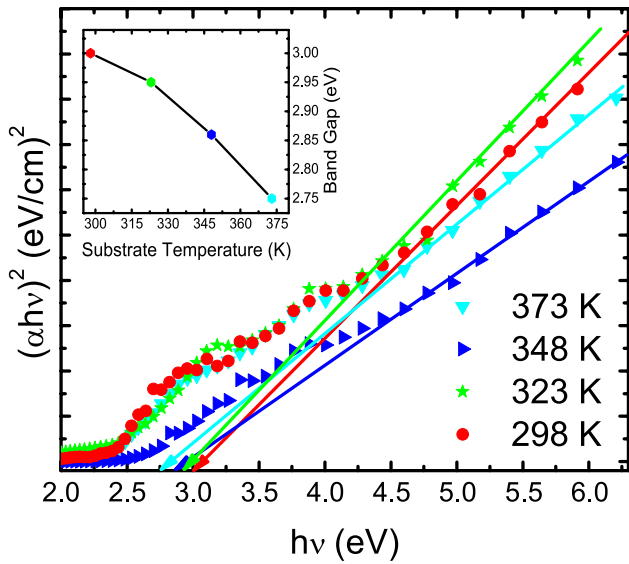
Fig. 2 Variation of $(\alpha h\nu)^2$ with energy for all ZnSe thin films. Inset: variation of band gap for ZnSe films deposited at different substrate temperature

Fig. 3 Temperature dependence of dark conductivity and *I–V* curves (inset) for all ZnSe thin films

eV. The variation of band gap for ZnSe films has been represented in Fig. 2 inset. The optical gap energy was reported to reduce from 3.00 to 2.75 eV when deposition temperature is enhanced from 298 to 373 K. This behavior can be understood by studying the quantum confinement effects in nanomaterials. To estimate the confinement in ZnSe thin films, the light hole exciton Bohr radius (a_B) has been calculated using

$$a_B = \frac{4\pi\varepsilon_0\varepsilon_r\hbar^2}{m_0 e^2}\left(\frac{m_e^* + m_h^*}{m_e^* m_h^*}\right), \tag{7}$$

where e is elementary charge, m_0 is free electron mass, ε_r is dielectric constant of ZnSe, m_e^* and m_h^* are effective masses of electron and hole, respectively. In present case of ZnSe, the values of $m_e^* = 0.149\,m_0$ and $m_h^* = 0.195\,m_0$ are considered from the full potential linearized plane wave (LAPW) method [37] and ε_r is considered to be 9.20 [38]. The value of a_B has been calculated to be 6 nm for light holes. The value of a_B is comparable to L in ZnSe thin films so we can expect weak confinement. Tan et al. [39] proposed that the shift in absorption edge can be attributed to the polycrystalline nature of materials. In polycrystalline materials, there is an increase of extended localization in the conduction and valence bands leading to blue shift in absorption edge [39]. In present case, the main reasons of blue shift are surface roughness and polycrystalline nature of ZnSe nanocrystallites along with weak quantum confinement. Khairnar et al. [40] observed an increase in optical band gap with the thickness of thermally evaporated ZnSe thin films. They suggested that films having small thickness are strained to a
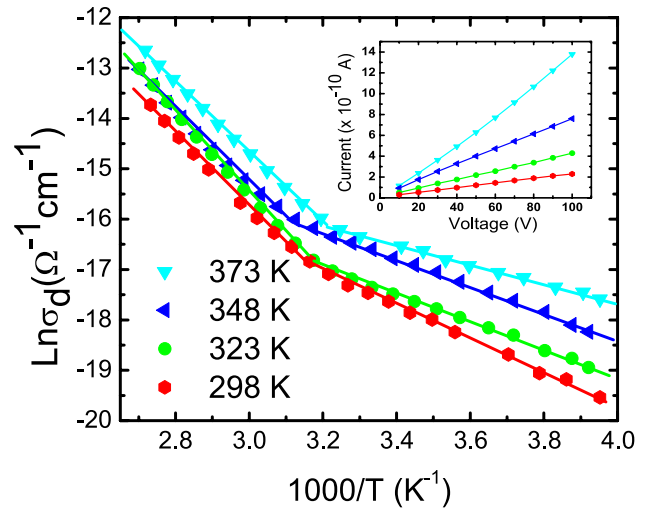
greater extent and have smaller crystallite size leading to highly absorbing films.

The refractive index of a semiconductor with energy gap E_g can be calculated using relation [1]

$$n = n_0[1 + \alpha \exp(-\beta E_g)] \tag{8}$$

where $n_0 = 1.73$, $\alpha = 1.9017$ and $\beta = 0.539\,(\text{eV})^{-1}$ are various constants for ZnSe at room temperature. The value of refractive index (calculated using Eq. 8) increases from 2.38 to 2.48 when deposition temperature is increased from 298 to 373 K (Table 3). The values of n have been used to calculate valence electron plasmon energy using relation $\hbar\omega_p = k_1 e^{-k_2 n}$, where constants $k_1 = 22.079$ and $k_2 = 0.1779$ for ZnSe has been considered from [41]. The Fermi energy (E_f) has been calculated using $0.2947(\hbar\omega_p)^{4/3}$. The crystal ionicity ($f_i$) has been calculated using Tubb relation [42] after some modifications [33] using

$$f_i = \left[\frac{1 - \frac{E_g}{4E_f}}{n^2 - 1}\right]^{\frac{1}{2}} \tag{9}$$

The degree of ionicity, in present case, has been found in the range 0.425–0.446 (Table 3).

The information about the contact type and electrode to crystallites contact formation can be obtained from *I–V* measurements. *I–V* characteristics of all the samples have been measured at room temperature and represented in Fig. 3 inset. Clearly, all the samples show linear Ohmic behaviour. The variation of conductivity (σ) with temperature can be represented by Arrhenius equation

$$\sigma = \sigma_0 \exp\left(\frac{-\Delta E}{k_B T}\right) \qquad (10)$$

where ΔE represents activation energy and k_B symbolizes Boltzmann's constant. The dark conductivity (σ_d) is temperature dependent and this variation has been presented in Fig. 3. There are two linear portions in $\ln\sigma_d$ versus 1000/T plots. A smaller slope is observed in temperature range of 250–315 K and a larger slope in range of 316–366 K. The room temperature values of σ_d are represented in Table 2. The activation energy in dark (ΔE_d) is estimated utilizing the slopes of Fig. 3 (Table 2). There is an increase in conductivity from 2.19×10^{-8} to 6.59×10^{-8} Ω^{-1}cm^{-1} as the deposition temperature is increased from 298 to 373 K (size increases). The activation energy at lower temperatures (250–315 K) is significantly lower than the activation energy at higher temperatures (316–366 K). The values of activation energies in higher temperature range indicate thermally activated band to band transitions [43]. The lower values of activation energy for lower temperatures indicate hopping as the most probable mechanism of the transport. Recently, similar results have been reported for ZnS$_x$Se$_{1-x}$ thin films [43]. To study the hopping conduction in lower temperature range, Mott model [44] can be utilised. According to Mott's variable-range hopping (VRH) model, the temperature dependance of conductivity is given by the equation [45, 46]:

$$\sigma = \frac{\sigma_{0M}}{T^{1/2}} \exp\left(-\frac{T_M}{T}\right)^{1/4} \qquad (11)$$

with Mott parameters σ_{0M} and T_M given by

$$\sigma_{0M} = \frac{3e^2 \nu_{ph}}{2}\left(\frac{N(E_F)}{2\pi\alpha_M k_B T}\right)^{1/2} \qquad (12)$$

$$T_M = \frac{\lambda\alpha_M^3}{k_B N(E_F)} \qquad (13)$$

where T_M is Mott temperature (degree of disorder), e is electronic charge, ν_{ph} is phonon frequency depending upon electron-phonon interaction and is a constant [45], $N(E_F)$ is density of states at Fermi level, α_M is coefficient of wave-function and λ is a constant.

To check the conduction mechanism in low temperature range, the variation of $\ln(\sigma T^{1/2})$ with $T^{-1/4}$ has been studied (Fig. 4). The linear behaviour of these plots suggest an electron transport by hopping among localized states. In polycrystalline materials, the VRH conduction process exists in the grain boundaries, in temperature range at which the carriers do not have sufficient energy to cross the potential barrier and to transfer themselves into grain by the process of thermionic emission [47]. However, hopping in this case takes place due to the transfer of the charge carriers from a charged trap state to a neutral trap state [48]. Hence, the conduction mechanism at low temperature can be attributed to the hopping mechanism of the charge carriers. Above results suggest that good quality ZnSe films can be synthesized at elevated substrate temperatures. The conductivity is observed to be dependent on crystallite size. It can be suggested that the increase in conductivity, for depositions done at elevated temperatures, is due to decrease in scattering
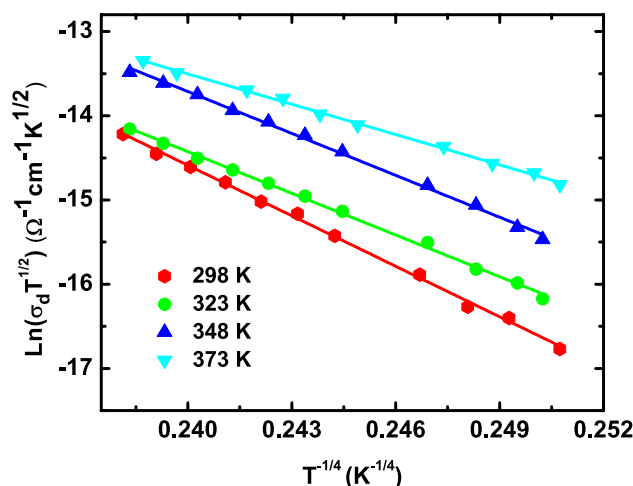

Fig. 4 The plot of $\ln(\sigma_d T^{1/2})$ versus $T^{-1/4}$ for all ZnSe thin films

Table 2 Dark conductivity (σ_d), photoconductivity (σ_{ph}), dark-activation energy (ΔE_d), photo-activation energy (ΔE_{ph}), and carrier life time ($(\ln \tau_d)_{t=0}$) for all ZnSe thin films

Substrate temp. (K)	σ_d [298 K] (Ω^{-1}cm^{-1})	($\Delta E_d \pm 0.01$) (eV)		σ_{ph} [298 K] (Ω^{-1}cm^{-1})	($\Delta E_{ph} \pm 0.01$) (eV)	$(\ln \tau_d)_{t=0}$ (s)
		LTR	HTR			
298	$(2.19 \pm 0.02) \times 10^{-8}$	0.28	0.63	$(9.42 \pm 0.02) \times 10^{-7}$	0.22	1.6
323	$(2.90 \pm 0.02) \times 10^{-8}$	0.24	0.71	$(2.22 \pm 0.02) \times 10^{-6}$	0.15	1.5
348	$(5.16 \pm 0.02) \times 10^{-8}$	0.23	0.63	$(6.10 \pm 0.02) \times 10^{-6}$	0.18	1.3
373	$(6.59 \pm 0.02) \times 10^{-8}$	0.17	0.60	$(1.29 \pm 0.02) \times 10^{-5}$	0.08	1.0

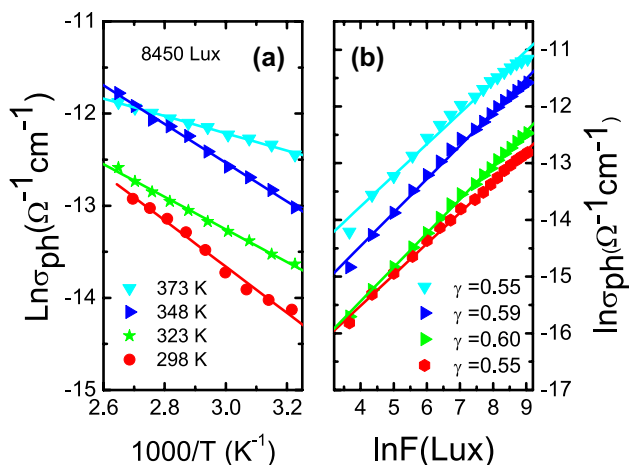LTR and HTR represent low and high temperature range, respectively

Fig. 5 a Temperature and **b** intensity dependence of photo conductivity for all ZnSe thin films

Fig. 6 a Rise and decay of photocurrent measured at 298 K and **b** plots of $\ln\tau_d$ versus $\ln t$ for all ZnSe thin films

at surface and also at grain boundaries (due to increase in crystallite size).

The photocurrent (I_{ph}) is the difference between the current measured after illuminance and current measured in dark (I_d). Figure 5a represents the variation of photoconductivity (σ_{ph}) with temperature. The values of σ_{ph}, at room temperature, have been represented in Table 2. σ_{ph} increases with increase in crystallite size. The dark activation energy is much higher than photo activation energy from 315 to 366 K range. The steady state photoconduction has been found to be intensity (F) dependent (Fig. 5b). This dependence can be presented by a power law $\sigma_{ph} \propto F^\gamma$, with $0.5 \leq \gamma \leq 1.0$. Rose [49] suggested that for γ values between 0.5 and 1.0 one can consider that there are continuous trap levels distribution in the energy gap. In our films, the values of γ ranges from 0.55 to 0.60. Due to this type of distribution, the recombination mechanism in ZnSe is bimolecular [50] and recombination rate varies proportionally with concentration of holes.

Figure 6a represents the time dependence of I_{ph} for ZnSe thin films. All thin films show a persistent photocurrent, which is a common feature of chalcogenides [22, 51]. For the quantitative analysis of decay rate, the time constant for decay (τ_d) is calculated for all samples using [52]

$$\tau_d = -\left[\frac{1}{I_{ph}}\frac{dI_{ph}}{dt}\right]^{-1} \tag{14}$$

The slopes of I_{ph} versus time plots, at various times, have been used to calculate the values of τ_d. These values are time dependent confirming that the current decays non-exponentially. The variation of $\ln\tau_d$ with $\ln t$, at room temperature (298 K) and intensity 8450 Lux, has been presented in Fig. 6b. The carrier life time has been obtained by
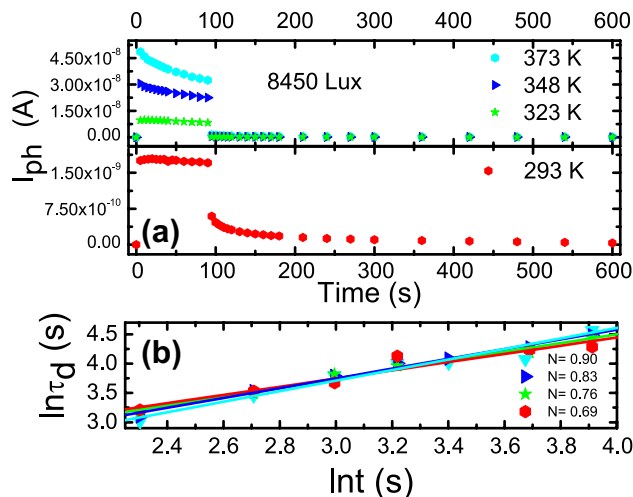
extrapolation of the curves at t = 0 [53]. These values have been presented in Table 2. The plots of Fig. 6b obey the power law $t^{-d\left(\frac{\ln\tau_d}{\ln t}\right)}$, where the quantity $d\left(\frac{\ln\tau_d}{\ln t}\right)$ can be termed as N. The values of N have been calculated from Figure and are represented there. The values of carrier life time in these films indicate that gap states are present near the mobility edge. The decrease of carrier life time with rise in deposition temperature indicates the lowering of mobility edge.

The electron transfer behaviour in all ZnSe thin films is influenced by their structural behaviour and impurities [47], so the conduction mechanism is successfully explained using different theories of Seto, Baccarani, Seager and Gastner developed for polycrystalline films [21, 54–58]. The details of the mechanism is described elsewhere [59]. The concentration of impurities (N_D), can be calculated using

$$E_b = \frac{e^2 L^2 N_D}{8\varepsilon_r} \tag{15}$$

where E_b is barrier potential, e is charge on an electron, L is crystallite size and ε_r is dielectric constant (low frequency). The variation of conductivity with temperature (T) can be utilized to calculate surface states concentration (N_t) using

$$\sigma_f = e^2 L^2 N_c N_D v \left[2k_B T (N_t - L N_D)\right]^{-1} \exp\left(-\frac{\Delta E_d}{k_B T}\right) \tag{16}$$

where N_c represents the effective state density. In our case, the value of ε_r is considered to be 9.20 [38]. The values of E_b, N_t and N_D have been calculated using Eqs. (15) and (16) (Table 3). The decrease in values of N_t and N_D with

Table 3 Representation of optical gap (E_g), refractive index (n), ionicity (f_i), barrier height (E_b), impurity concentration (N_D) and surface states density (N_t) for all ZnSe thin films

Substrate temp. (K)	($E_g \pm 0.01$) (eV)	n	f_i	($E_b \pm 0.01$) (eV)	N_D (cm^{-3})	N_t (cm^{-2})
298	3.00	2.38	0.446	0.28	3.18×10^{20}	2.15×10^{14}
323	2.95	2.40	0.442	0.24	2.30×10^{20}	1.68×10^{14}
348	2.86	2.43	0.436	0.23	1.98×10^{20}	1.53×10^{14}
373	2.75	2.48	0.425	0.17	1.26×10^{20}	1.05×10^{14}

deposition at higher temperature is quite evident as there is decrease in surface to volume ratio with increasing size of crystallites.

4 Conclusions

Polycrystalline ZnSe thin films having hexagonal structure are prepared by inert gas condensation at substrate temperatures varying from 298 to 373 K. Films deposited at lower substrate temperatures are orientated along the (002) and films deposited at higher temperatures are oriented along (102) planes. The crystallite size, dislocation density, microstrain and texture coefficient are found to be dependent on deposition temperature. Polycrystalline nature and weak confinement effects lead to shift in the absorption edge towards higher wavelengths and this shift is more prominent for depositions done at higher temperatures. The dark- and photo-conductivity of these thin films have larger values for depositions done at higher temperatures. The carrier life time has minimum value at the higher temperature deposition. Photo-conductivity measurements reveal that there are localized states with a continuous distribution and a slow decay of photocurrent is observed. This indicates that there are deeper localised states in these films. These results also indicate that deposition temperature has remarkable effect on different parameters of ZnSe thin films. Good quality ZnSe thin films can be obtained for depositions done at higher temperatures in the presence of Ar.

References

1. S.K. Tripathy, A. Pattanaik, Opt. Mater. **53**, 123 (2016)
2. J.M. McHale, A. Auroux, A.J. Perrota, A. Navrotsky, Science **277**, 788 (1997)
3. B.G. Yacobi, *Semiconductor Materials: An Introduction to Basic Principles* (Kluwer Academic Publishers, Dordrecht, 2004)
4. S. Prasad, H. Schumacher, A. Gopinath, *High Speed Electronics and Optoelectronics: Devices and Circuits* (Cambridge University Press, Cambridge, 2009)
5. C.H. Hsiao, S.J. Chang, S.B. Wang, S.C. Hung, S.P. Chang, T.C. Li, W.J. Lin, B.R. Huang, Superlattices Microstruct. **46**, 572 (2009)
6. W. Sukkabot, Superlattices Microstruct. **75**, 739 (2014)
7. L. Wang, R. Chen, Z.-F. Ren, C.-W. Ge, Z.-X. Liu, S.-J. He, Y.-Q. Yu, C.-Y. Wu, L.-B. Luo, Nanotechnology **27**, 215202 (2016)
8. S.E. Al Garni, A.F. Qasrawi, Funct. Mater. Lett. **9**(2), 1650019 (2016)
9. G.M. Lohar, S.T. Jadhav, M.V. Takale, R.A. Patil, Y.R. Ma, M.C. Rath, V.J. Fulari, J. Colloid Interface Sci. **458**, 136 (2015)
10. S. Ferahtia, S. Saib, N. Bouarissa, S. Benyettou, Superlattices Microstruct. **67**, 88 (2014)
11. X. Zhang, D. Wang, M. Beres, L. Liu, Z. Ma, P.Y. Yu, S.S. Mao, Appl. Phys. Lett. **103**, 082111 (2013)
12. D. Shikha, V. Mehta, J. Sharma, R.P. Chauhan, J. Mater. Sci. Mater. Electron. **28**(12), 8359 (2017)
13. H.H. Yudar, S. Pat, S. Korkmaz, S. Ozen, Y. Şenay, J. Mater. Sci. Mater. Electron. **28**(3), 2833 (2017)
14. B. Feng, J. Cao, D. Han, H. Liang, S. Yang, X. Li, J. Yang, Mater. Sci. Semicond. Process. **27**, 865 (2014)
15. C.I. Nweze, A.J. Ekpunobi, Afr. Rev. Phys. **10**(1), 105 (2015)
16. R. Indirajith, M. Rajalakshmi, K. Ramamurthi, M.B. Ahamed, R. Gopalakrishnan, Ferroelectrics **467**, 13 (2014)
17. M. Shakir, G.Bhagavannarayana Shartha, M.A. Wahab, Chalcogenide Lett. **8**(7), 435 (2011)
18. F. Shaik, W. Zhang, W. Niu, Langmuir **33**(13), 3281 (2017)
19. M. Maicu, R. Schmittgens, D. Hecker, D. Gloß, P. Frach, G. Gerlach, J. Vac. Sci. Technol. A **32**(2), 02B113 (2014)
20. I.V. Chepkasov, Y.Y. Gafner, S.L. Gafner, S.P. Bardahanov, Phys. Metals Metallogr. **117**, 1003 (2016)
21. J.Y.W. Seto, J. Appl. Phys. **46**, 5247 (1975)
22. A. Thakur, V. Sharma, G.S.S. Saini, N. Goyal, S.K. Tripathi, J. Phys. D **38**, 1959 (2005)
23. P. Kumar, R. Thangaraj, J. Phys. Condens. Matter **21**, 375102 (2009)
24. JCPDS file number 00-015-0105
25. N. Fujimura, T. Nishihara, S. Goto, J. Xua, T. Ito, J. Cryst. Growth **130**(1–2), 269 (1993)
26. V.D. Mote, Y. Purushotham, B.N. Dole, J. Theor. Appl. Phys. **6**(6), 1 (2012)
27. J. Sharma, H. Singh, T. Singh, J. Sci. Adv. Mater. Devices **2**(4), 432 (2017)
28. K. Reichelt, X.T. Jiang, Thin Solid Films **191**, 91 (1990)
29. I.A. Ovidko, Rev. Adv. Mater. Sci. **1**, 61 (2000)
30. B.E. Warren, B.L. Averbach, J. Appl. Phys. **21**, 596 (1959)
31. A. Islam, C. Das, S. Choudhury, M. Sharmin, T. Begum, Eur. Sci. J. **10**(15), 241 (2014)
32. R.K. Pathak, S. Bais, Int. J. Adv. Eng. Technol. **7**(4), 1300 (2014)
33. G.S. Thool, A.K. Singh, R.S. Singh, A. Gupta, M.A.B.H. Susan, J. Saudi Chem. Soc. **18**(5), 712 (2014)
34. T. Mahalingam, V.S. John, L.S. Hsu, J. New Mater. Electrochem. Syst. **10**(1), 9 (2007)

35. J.I. Pankove, *Optical Processes in Semiconductors* (Prentice-Hall, Englewood Cliffs, 1971)
36. J. Sharma, G. Singh, A. Thakur, G.S.S. Saini, N. Goyal, S.K. Tripthi, J. Optoelectron. Adv. Mater. **7**, 2085 (2005)
37. A. Rubio-Ponce, D. Olguin, I. Hernandez-Calderon, Superficies y Vacio **16**(2), 26 (2003)
38. T.S. Moss, M. Balkanski (eds.), *Handbook on Semiconductors: Optical Properties of Semiconductors* (Elsevier, Amsterdam, 1994)
39. S.T. Tan, B.J. Chen, X.W. Sun, X. Hu, X.H. Zhang, S.J. Chua, J. Cryst. Growth **281**, 571 (2005)
40. U. Khairnar, S. Behere, P. Pawar, Mater. Sci. Appl. **3**(1), 36 (2012)
41. R.R. Reddy, Y.N. Ahammed, P.A. Azeem, K.R. Gopal, B.S. Devi, T.V.R. Rao, Def. Sci. J. **53**, 239 (2003)
42. M.R. Tubb, Phys. Status Solid. **41**, k61 (1970)
43. M. Popa, I. Tiginyanu, V. Ursaki, Roman. J. Phys. **62**, 602 (2017)
44. N.F. Mott, J. Non Cryst. Sol. **1**, 1 (1968)
45. N.F. Mott, E.A. Davis, *Electronic Processes in Non-crystalline Materials*, 2nd edn. (Clarendon Press, Oxford, 1979)
46. M.Z. Ansari, N. Khare, J. Appl. Phys. **117**, 025706 (2015)
47. K. Sharma, A.S. Al-Kabbi, G.S.S. Saini, S.K. Tripathi, Appl. Phys. A **108**, 911 (2012)
48. A.A. Abu-Sehly, M.I. Abd-Elrahman, J. Phys. Chem. Solids **63**, 163 (2002)
49. A. Rose, *Concepts in Photoconductivity and Allied Problems* (Interscience, New York, 1963)
50. A. Thakur, V. Sharma, P.S. Chandel, N. Goyal, G.S.S. Saini, S.K. Tripathi, J. Mater. Sci. **41**(8), 2327 (2006)
51. M. Igalson, Solid State Commun. **44**, 247 (1982)
52. W. Fuhs, D. Meyer, Phys. Status Solid. **24**, 275 (1974)
53. D.P. Padiyan, A. Marikani, K.R. Murali, Cryst. Res. Technol. **35**, 949 (2000)
54. K.L. Chopra, *Thin Film Phenomena* (McGraw-Hill, New York, 1969)
55. G. Harbeke (ed.), *Polycrystalline Semiconductors: Physical Properties and Applications* (Springer, Berlin, 1985)
56. L.L. Kazmerski (ed.), *Polycrystalline and Amorphous Thin Films and Devices* (Academic Press, New York, 1980)
57. G. Baccarani, B. Ricco, G. Spandini, J. Appl. Phys. **49**, 5565 (1978)
58. C.H. Seager, T.G. Gastner, J. Appl. Phys. **49**, 3879 (1978)
59. J. Sharma, S.K. Tripathi, Physica B **406**, 1757 (2011)